

# Molecular-Kinetic Simulations of Escape from the Ex-planet and Exoplanets: Criterion for Transonic Flow

Robert E. Johnson<sup>1,2</sup>, Alexey N. Volkov<sup>1</sup> and Justin T. Erwin<sup>1</sup>

<sup>1</sup> Engineering Physics, University of Virginia, Charlottesville, VA 22904-4745, USA

<sup>2</sup> Physics Department, New York University, NY 10003-6621, USA

## Abstract:

The equations of gas dynamics are extensively used to describe atmospheric loss from solar system bodies and exoplanets even though the boundary conditions at infinity are not uniquely defined. Using molecular-kinetic simulations that correctly treat the transition from the continuum to the rarefied region, we confirm that the energy-limited escape approximation is valid when adiabatic expansion is the dominant cooling process. However, this does not imply that the outflow goes sonic. Rather large escape rates and concomitant adiabatic cooling can produce atmospheres with subsonic flow that are highly extended. Since this affects the heating rate of the upper atmosphere and the interaction with external fields and plasmas, we give a criterion for estimating when the outflow goes transonic in the continuum region. This is applied to early terrestrial atmospheres, exoplanet atmospheres, and the atmosphere of the ex-planet, Pluto, all of which have large escape rates.

## Introduction

Rapid atmospheric escape is often described as a gas that goes sonic, sometimes called blow-off (Hunten 1982), a process that accounts for certain isotope ratios on terrestrial planets. Transonic models have also been used to describe rapid escape from exoplanets (e.g., Murray-Clay et al. 2009) and from Pluto (e.g., Strobel 2008). However, we recently showed that this model for Pluto gave an incorrect upper atmospheric structure (Tucker et al. 2012; Erwin et al. 2013).

In simulating rapid escape using continuum gas dynamics, the Jeans expressions at the exobase have been applied for the uncertain boundary conditions at infinity (e.g., Tian et al. 2008). More often, a sonic point is assumed to occur at some altitude, above which the density and temperature dependence can be simply characterized (Parker 1964a,b). The so-called energy-limited escape rate, extensively applied to exoplanet atmospheres (e.g., Lammer et al. 2009), is often assumed to imply that sonic boundary conditions are applicable (e.g., Erkaev et al. 2012). Here we use molecular-kinetic simulations to show that is not the case.

We briefly review the continuum and molecular-kinetic models, and then present results of our simulations. These test the applicability of the energy-limited escape rate and our proposed criterion for determining whether sonic or kinetic upper boundary conditions are applicable. The results are applied to escape from Pluto, early terrestrial planet, and exoplanet atmospheres.

## Models

We describe escape from a one-dimensional (1D), steady state, single component atmosphere as illustrative, leaving out thermal transport by horizontal flow. For radial

44 distance  $r$ , flow speed  $u$ , number density  $n$ , temperature  $T$ , pressure  $p = nkT$ , and escape  
 45 rate  $\Phi = 4\pi r^2 n u = \text{const}$ , the momentum and energy equations are often used ignoring  
 46 viscosity:

$$47 \quad n \frac{d}{dr} (mu^2/2 - U) = - \frac{dp}{dr} \quad (1)$$

$$48 \quad \frac{d}{dr} \left[ \Phi (mu^2/2 + C_p kT - U) - 4\pi r^2 \kappa \frac{dT}{dr} \right] = 4\pi r^2 n q_a(r) \quad (2)$$

49 Here  $k$  is the Boltzmann constant,  $\kappa = \kappa(T)$  the thermal conductivity,  $C_p$  the specific  
 50 heat at constant pressure,  $m$  the molecular mass,  $U = U(r) = GMm/r$  the gravitational  
 51 energy ( $G$  the gravitational constant,  $M$  the planet's mass), and  $q_a(r)$  is the *net* heating  
 52 rate per molecule produced by incident photons or plasma particles, in which we include  
 53 radiative cooling. Knowing the density,  $n_0$ , and temperature,  $T_0$ , at a lower boundary,  
 54  $r = r_0$ , a unique solution requires two other conditions, typically at the upper boundary.  
 55 The gravitational energy is characterized by the Jeans parameter,  $\lambda(r) = U/kT$  and the  
 56 rarefaction by the Knudsen number,  $Kn(r) = l_c/H$ , the ratio of the mean free path of gas  
 57 molecules,  $l_c$ , to the scale height,  $H = -n/(dn/dr)$ . For an escaping gas at large  
 58 distances from the source, where free molecular flow occurs,  $H \rightarrow r/2$ ; in the hydrostatic  
 59 regime  $H \rightarrow r/\lambda(r)$ .

60 The Jeans expressions for the number,  $\Phi_J$ , and thermal,  $\langle E\Phi \rangle_J$ , escape rates have  
 61 been used as upper boundary conditions for Equations (1-2):

$$62 \quad \Phi_J = 4\pi r_x^2 n_x \sqrt{\frac{kT_x}{2\pi m}} (1 + \lambda_x) \exp(-\lambda_x) \quad (3a)$$

$$63 \quad \langle E\Phi \rangle_J = kT_x \Phi_J \left( \frac{1}{1+\lambda_x} + C_p - \frac{3}{2} \right) \quad (3b)$$

64 The subscript 'x' indicates quantities evaluated at the nominal exobase,  $r = r_x$ , where  
 65  $Kn(r_x) \approx 1$ , often assumed to be the upper boundary of the continuum region. When the  
 66 upper atmosphere heating rate is large, the equations are more often solved through a  
 67 sonic point,  $r = r_*$ , where  $u_* = c$  ( $c = \sqrt{\gamma kT/m}$  the sound speed,  $\gamma = C_p/C_V$ ,  $C_V$  the  
 68 specific heat per unit mass at constant volume). For  $r \gg r_*$  then  $n$  and  $T$  decay as power  
 69 laws (Parker 1964a,b). Unfortunately those continuum solutions for which Jeans escape  
 70 is applicable and those for which a sonic point is reached in the continuum region do not  
 71 simply track from one to the other as the heating rate increases.

72 Kinetic models *can* simulate both continuum ( $l_c \ll H$ ) and non-continuum  
 73 (transitional,  $l_c \sim H$ , and free molecular,  $l_c \gg H$ ) gas flows and can, therefore, describe  
 74 the change from Jeans-like to transonic escape. Since such simulations track particles in  
 75 the potential well of the body (or bodies) of interest, escape is a natural outcome. We  
 76 numerically implement a kinetic description of rarefied gas flow in an upper atmosphere  
 77 based on the Boltzmann kinetic equation using the direct simulation Monte Carlo  
 78 (DSMC) method (Bird 1994). In this method, the gas flow is represented by a large set of  
 79 representative atoms or molecules that are tracked subject to binary collisions and gravity  
 80 (Volkov 2011a,b). Heating of the atmosphere is implemented by scaling the thermal  
 81 velocities of the representative molecules according to the local energy deposition rate.

82 The lower boundary of the simulation region,  $r = r_0$ , is below the depth at which  
 83 the UV/EUV or plasma energy deposition occurs and  $Kn_0 \ll 1$ . Because the density  
 84 drops rapidly with increasing  $r$ , but escape occurs at large  $r$  where the density is low,  
 85 DSMC simulations starting at small  $Kn_0$  can require an enormous number of particles to  
 86 accurately describe escape. Therefore, we also use a hybrid continuum/kinetic model  
 87 (Tucker et al. 2012) in which the Equations (1-2) are solved at  $Kn < \sim 0.1 - 0.01$ , where  
 88 the gas is collisionally dominated, and the velocity and internal energy distributions are  
 89 reasonably well represented by Maxwellians, and then iteratively couple it to a DSMC  
 90 simulation in the rarefied region.

## 91 Heating

92 Parker (1964a,b) used Equations (1-2) to describe escape when the dominant heat  
 93 source is internal, as it is for expansion of the solar corona: i.e.,  $q_a(r) = 0$  for  $r > r_0$ .  
 94 This model was subsequently applied to planetary atmospheres primarily heated at  $r <$   
 95  $r_0$ . For Jeans parameters at  $r = r_0$  as large as  $\lambda_0 \sim 40$ , such models were assumed to  
 96 produce a transonic expansion, often referred to as ‘slow hydrodynamic escape’ (e.g.,  
 97 Strobel 2008). Although, rapid escape *can* occur for relatively large  $\lambda_0$  and  $Kn_0 \ll 1$ , for  
 98  $\lambda_0 > \sim (C_p + \gamma/2)$  the gas does not go sonic in the collision-dominated region and the  
 99 escape rate is a factor of a few larger than the Jeans rate (Volkov et al. 2011a,b). Ignoring  
 100 the thermal conductivity in Equation (2), this corresponds to when the enthalpy of fluid  
 101 particles becomes sufficient for a transonic, isentropic expansion starting at  $r_0$ . For  
 102 smaller  $\lambda_0$  a non-equilibrium region, a Knudsen layer, forms above  $r = r_0$  and there is  
 103 a steep transition with decreasing  $\lambda_0$  to supersonic escape at  $\lambda_0 \sim 2.1$  and  $\sim 2.8-3.5$  for  
 104 monatomic and diatomic gases respectively (Volkov & Johnson 2013).

105 In an upper atmosphere heated by short wavelength radiation, or by incident  
 106 plasma particles, escape is driven by the energy absorbed. Energy absorbed below  
 107  $Kn \sim 0.1$  is typically converted to heat using an efficiency,  $\varepsilon$ , that depends on the  
 108 radiation type and atmospheric composition. The heating rate is either directly calculated  
 109 or a value of  $\varepsilon$  is estimated: often a constant ( $\sim 0.15 - 0.4$ ) up to the exobase where it  
 110 goes to zero. Typically the gas-dynamic equations for exoplanet or early terrestrial  
 111 atmospheres are then solved with Jeans-like or sonic upper boundary conditions. As  
 112 discussed below, we used a hybrid continuum/DSMC model to describe escape from  
 113 Pluto heated by the solar UV/EUV and a DSMC model to describe escape from an  
 114 atmosphere in which, the heating is assumed to occur in a narrow layer.

## 115 Energy Limited Escape

116 Because thermal conduction in the upper atmosphere is inefficient, adiabatic  
 117 cooling by escape or horizontal transport often dominates (e.g., Erwin et al. 2013). For a  
 118 *globally averaged* heating rate and adiabatic cooling, integration of Equation (2) gives a  
 119 rough upper bound to the escape rate,  $\Phi_{EL}$  (e.g., Lammer et al. 2009):

$$120 \quad \Phi_{EL} \approx Q_{net} / (U - C_p kT - mu^2/2) \Big|_{r=r_0}. \quad (4)$$

121 Here  $r_0$  is below the heated region, above which adiabatic cooling dominates;  $Q_{net} =$   
 122  $4\pi \int_{r_0}^{\infty} r^2 q_a(r) dr$  is the integrated heating+radiative cooling rate. This expression is  
 123 often referred to as the energy-limited rate, although Watson et al. (1981) discussed a  
 124 related quantity. For  $r_0$  deep in the gravitational well and  $\lambda_0 \gg C_p$ , Equation (4) is often  
 125 approximated as

$$126 \quad \Phi_{EL} \approx Q_{net}/U(r_0). \quad (5)$$

127 Assuming a small fraction of  $Q_{net}$  is deposited for  $Kn > \sim 0.1$ , so non-thermal escape  
 128 processes (Johnson et al. 2008) can be ignored, we showed that UV/EUV heating of  
 129 Pluto's atmosphere resulted in an escape rate very close to that in Equation (5), *but* the  
 130 gas did not go sonic below the exobase. Rather, a large expansion of the upper  
 131 atmosphere occurred (Tucker et al. 2012; Erwin et al. 2013). Similarly, Tian et al. (2008)  
 132 found that above a heating threshold, the atmosphere rapidly expanded and the escape  
 133 rate increased with increasing EUV heating, consistent with energy-limited escape, even  
 134 though the gas remained subsonic. Therefore, the energy limited escape rate is *not*  
 135 contingent on the flow going sonic below the exobase. If the heating rate is increased to  
 136 the point where the atmosphere does go sonic in the continuum region, energy limited  
 137 escape can still apply if one accounts for the large  $u$ , enhanced radiative cooling,  
 138 recombination in an ionized atmosphere, etc. (e.g., Murray-Clay et al. 2009).

### 139 **Criteria for Transonic Solutions**

140 Since the isentropic approximation and energy-limited escape are applicable to  
 141 both sub-sonic and transonic rapid outflows, we use the Mach number,  $Ma =$   
 142  $u/\sqrt{\gamma kT/m}$ , and rewrite Equation (5):

$$143 \quad Q_{net} \approx 4\pi r^2 n Ma \sqrt{\frac{\gamma U(r)}{\lambda m}} U(r_0) \quad (6)$$

144 Because the boundary conditions for sub-sonic and transonic solutions differ, it is  
 145 important to be able to estimate the minimum value of  $Q_{net}$  required to apply sonic  
 146 boundary conditions, which we will call  $Q_c$ . Assuming the sonic point,  $r = r_*$ , occurs in  
 147 the continuum region, the flow can be effectively approximated by the isentropic model:

$$148 \quad 2mc^2(r_*) = U(r_*) + (\gamma - 1) \frac{r_* q(r_*)}{u(r_*)}. \quad (7)$$

149 (e.g., Murray-Clay et al. 2009). For  $q(r_*) \approx 0$  Equation (7) reduces to  $\lambda_* \approx 2\gamma$  and  
 150 transonic escape occurs when  $Ma > 1$  in Equation (6) giving:

$$151 \quad Q_{net} > Q_c \approx 4\pi r_*^2 n_* \sqrt{\frac{U(r_*)}{2m}} U(r_0), \quad (8)$$

152 Below we estimate  $Q_c$  and test it.

153 We first consider a narrow heating layer located at  $r = r_a > r_0$  with  $Kn(r_a) \ll 1$ ,  
 154 as in Watson et al. (1981) and McNutt (1989), and give an approximate analytic solution  
 155 to Equations (1-2) in the Appendix. For this case, we performed DSMC simulations for a

156 monatomic gas of hard spheres with  $\lambda_0 = 10$ ,  $Kn_0 = 10^{-3}$ ,  $r_a/r_0 = 1.1$ . For  $Q_{net} =$   
 157  $0$ , we showed earlier that these conditions correspond to enhanced Jeans-like escape with  
 158  $\Phi \approx 1.6\Phi_J$  (Volkov et al. 2011a,b). Increasing  $Q_{net}$  to find when the outflow goes sonic  
 159 in the continuum regime, it is seen in Figure 1 that for  $Q_{net} \gg 0$  a non-equilibrium layer  
 160 forms near  $r_a$  in which the parallel and perpendicular components of temperature differ.  
 161 For small  $Kn(r_a)$  the flow properties in this layer are analogous to those in the Knudsen  
 162 layer discussed above for heating below  $r_0$ . Near  $r_a$  the density and temperature change  
 163 dramatically but the pressure from  $r_0$  to  $\sim r_a$  can be estimated from the hydrostatic  
 164 approximation. When the outflow goes sonic, a pressure drop occurs from  $\sim r_a$  to  $r_*$ :  
 165  $P_c = p_*/p_a$  (Volkov and Johnson 2013). Since the transition layer is narrow,  $r_* \approx r_a$ , we  
 166 rewrite Equation (8) using values at  $r_0$ :

$$167 \quad Q_{net} > Q_c \approx \langle E\Phi \rangle_0 [2\gamma\sqrt{\pi\lambda_0} \left(\frac{r_a}{r_0}\right)^{\frac{5}{2}} P_c \frac{p_a}{p_0}] \quad (9)$$

168 Here  $\langle E\Phi \rangle_0 = 4\pi r_0^2 n_0 k T_0 \sqrt{kT_0/(2\pi m)}$  is the upward Maxwellian energy flux of  
 169 molecules leaving the source at  $r = r_0$ . When the effects of thermal conduction are small  
 170 relative to adiabatic cooling, then Equation (9) can be derived from the analytic  
 171 expression in the Appendix. The barometric equation gives  $p_a/p_0 \approx \exp[\lambda_0(r_0/r_a - 1)]$   
 172 with  $P_c$  depending on the number of degrees of freedom:  $\sim 0.4$  for a monatomic gas. From  
 173 Figure 1, the transition to supersonic flow occurs for  $0.46 < Q_{net}/Q_c < 0.67$ . Due to the  
 174 above approximations, Equation (9) overestimates  $Q_c$  by about a factor of two. It is also  
 175 seen in Figure 1c that  $n(r)$  for the subsonic solution increases slowly for  $r \gg r_a$ ,  
 176 resulting in a significantly expanded atmosphere, but  $n(r)$  for the transonic solution in  
 177 Figure 1e roughly decreases as a power law consistent with transonic escape.  
 178

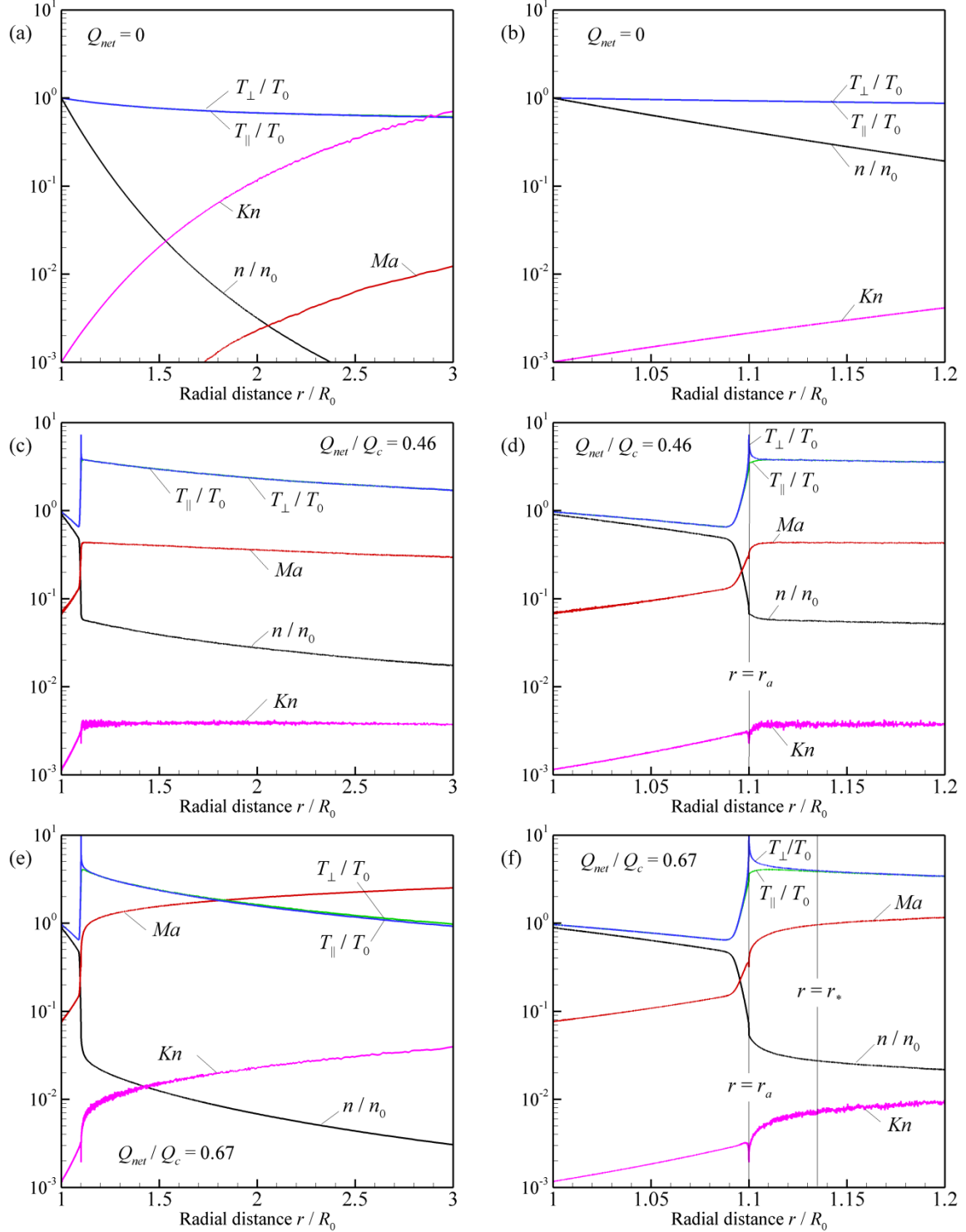


**Figure 1.** DSMC simulations: a monatomic gas of hard spheres at  $\lambda_0 = 10$ ,  $Kn_0 = 10^{-3}$  heated at  $r_a/r_0 = 1.1$ . Scaled density,  $n/n_0$  (black), parallel,  $T_{\parallel}/T_0$  (green), and perpendicular,  $T_{\perp}/T_0$  (blue), temperatures, and local Mach (red) and Knudsen (magenta) numbers for  $Q_{net}/Q_c = 0$  (a,b; Jean-like escape),  $=0.46$  (c,d; subsonic;  $\Phi/\Phi_{EL} = 0.87$ ), and  $=0.67$  (e,f; transonic at  $r_a/r_0 = 1.13$ ;  $\Phi/\Phi_{EL} = 0.65$ ). Lines: Heated and sonic surfaces.

180 As important, the escape rate in Figure 1 is seen to increase dramatically above  
 181  $Q_{net} = 0$  and becomes close to  $\Phi_{EL}$  in Equation (5) in the *subsonic* regime as seen in  
 182 Figure 2. Although  $\Phi$  does not change significantly in the transition to transonic escape, a  
 183 steep increase *is* seen in the thermal+flow energy removed,  $\langle E \Phi \rangle$ . It is also seen that  
 184 additional heating primarily increases the average kinetic energy of escaping molecules  
 185 so that Equation (5) becomes a poor approximation if  $Q_{net} \gg Q_c$ .

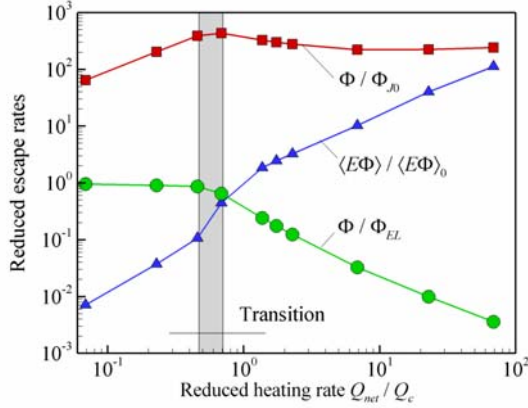


**Figure 2.** Number,  $\Phi$  [green circles, red squares] and energy,  $\langle E\Phi \rangle$  [blue triangles] escape rates vs.  $Q_{net}/Q_c$  calculated as for Figure 1: Scaled to  $\Phi_{EL}$  from Equation (5),  $\Phi_{J0}$  from Equation (3a) evaluated at  $r_0$ , and the energy flux of molecules across  $r_0$ ,  $\langle E\Phi \rangle_0 = 4\pi r_0^2 n_0 k T_0 \sqrt{k T_0 / (2\pi m)}$ . Rectangle indicates transition from subsonic to supersonic flow below the exobase; for smaller  $Q_{net}/Q_c$ ,  $\Phi \sim \Phi_{EL}$ ; for larger  $Q_{net}/Q_c$ , additional heating increases average energy of escaping molecules  $\langle E\Phi \rangle / \Phi$ .

186 We now consider more realistic heating profiles. In order to apply sonic boundary  
 187 conditions in Equations (1-2),  $Kn(r_*)$  must be in the continuum region below some  
 188 maximum,  $Kn_m$ : i.e.,  $Kn(r_*) = l_{c*}/H_* < Kn_m$ . Using  $H_* \sim r_*/\lambda_*$  and  $l_{c*} = 1/(c_c \sigma_c n_*)$ ,  
 189 where  $c_c$  is determined by the energy dependence of the total collision cross section  $\sigma_c$   
 190 (e.g.,  $c_c = \sqrt{2}$ ,  $\sigma_c = \pi d^2$  for the gas of hard sphere molecules of diameter  $d$ ), then  
 191  $2\gamma/(c_c r_* \sigma_c n_*) < Kn_m$ . From Equation (8), we estimate  $Q_c$  when  $r_*$  occurs in the  
 192 continuum domain:

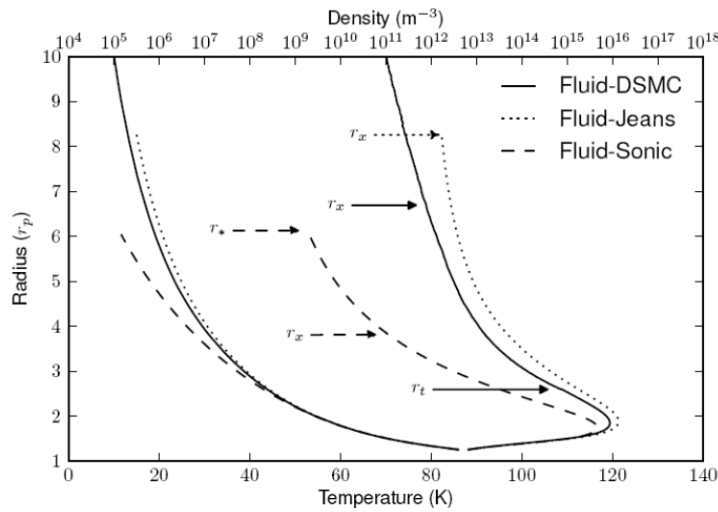
$$193 \quad Q_{net} > Q_c \approx 4\pi r_* \frac{\gamma}{c_c \sigma_c Kn_m} \sqrt{\frac{2U(r_*)}{m}} U(r_0), \quad (10)$$

194 where  $r_0 < r_* < r_x$ . When there is a sharp change in the gas properties, as for the heated  
 195 layers discussed above, then  $Kn_m < \sim 0.1$  (Volkov and Johnson 2013). However, if the  
 196 heat is primarily absorbed over a board range of  $r$  below  $r_x$ , then  $Kn_m \sim 1$  is sufficient.

197 It is seen in Equation 10 that  $Q_c$  does not *explicitly* depend on  $T_0$ , consistent with  
 198 simulations when  $\Phi$  is large. Because  $Q_c$  depends on the sonic point only via  $(r_*)^{1/2}$ , a  
 199 rough lower bound can be obtained by replacing  $r_*$  with the mean energy absorption  
 200 depth,  $r_a$  estimated from the absorption cross section,  $\sigma_a$ . More accurately, at threshold  
 201 the sonic point approaches  $r_x$  so that  $r_* \sim r_a [1 + (\sigma_a/c_c \sigma_c) \lambda_{ave}]$  where  $\lambda_{ave} \sim (\lambda_a +$   
 202  $2\gamma)/2$  slightly increasing  $Q_c$ . For a close-in exoplanet, tidal heating can be included

203 in  $U(r)$  and ion escape can dominate so that  $\sigma_c$  becomes large due to ion-neutral or ion-  
 204 ion collisions reducing  $Q_c$ .

205 For solar minimum, medium, and maximum conditions we simulated Pluto's  
 206 upper atmosphere at the New Horizons encounter using our hybrid fluid/kinetic model  
 207 ignoring the interaction with the solar wind and Charon, as well as non-thermal escape  
 208 (Erwin et al. 2013). For all three cases ( $Q_{net} = 0.38, 0.78, \sim 1.6 \times 10^8$  W) the atmosphere  
 209 became *highly* extended, but the flow remained subsonic *contrary to all* earlier models  
 210 (e.g., Strobel 2008) with the escape rate close to the energy-limited estimate in Equation  
 211 (4). It is seen in Figure 3 that at solar medium  $r_x$  is more than twice that obtained when  
 212 sonic boundary conditions are applied and, although the escape rate is large, using the  
 213 Jeans boundary conditions results a much better approximation to the upper atmosphere  
 214 structure.  
 215



216 **Figure 4.** Fluid simulations of Pluto's  $N_2$  atmosphere at 32Au at solar-medium; upper bc: (solid) fluid/  
 217 DSMC coupled at  $r_t, Kn = 0.1$ ;  $\Phi = 2.6 \times 10^{27}$ ; (dashed) transonic assumption:  $r_* > r_x$ ,  $\Phi = 2.5 \times 10^{27}/s$   
 218 (Strobel 2008); (dotted) Jeans bc from Equations (3a,b) at  $r_x \sim (7-8)r_p$ ;  $\Phi = 2.6 \times 10^{27}/s$ ;  $r_p = 1153$  km  
 219 Pluto's radius;  $r_0 = 1.25r_p$  roughly the visible extinction radius; parameters in VHS-LB model (Erwin et  
 220 al. 2013):  $m = 28$  amu,  $n_0 = 4 \times 10^{12} \text{ cm}^{-3}$ ,  $T_0 = 88.2$  K;  $U(r_0) = 2.8 \times 10^{-13}$  ergs;  $\lambda_0 = 23$ ;  $\gamma =$   
 221  $\frac{7}{5}$ ;  $\sigma_c \sim 9 \times 10^{-15} \text{ cm}^2$ ;  $Kn_0 \sim 10^{-6}$   
 222  
 223

224 For UV/EUV absorption at  $r_a \sim 1.5$  times Pluto's radius,  $r_p$ , using  $Kn_m \sim 1$  and  
 225  $r_* \sim r_a \sim r_0$ , Equation (9) gives  $Q_c > \sim 10 \times 10^8$ . This is *well above* the largest heating  
 226 rate ( $\sim 1.6 \times 10^8$  W) in Erwin et al. (2013). Therefore, Pluto's atmosphere at the New  
 227 Horizon encounter will be highly extended with an escape rate very close to the energy-  
 228 limited rate, but the flow in the continuum region will be sub-sonic.

229 In order to further test Equation (10), we performed DSMC simulations with a  
 230 distributed heating model in which, for simplicity, we used Beer's law along the radial  
 231 direction (Murray-Clay et al. 2009):  $q_a(r) = \varepsilon \sigma_a n(r) F_{UV/EUV} \exp(-\sigma_a N(r))$ , where  $\sigma_a$ ,  
 232  $\varepsilon$ , and  $F_{UV/EUV}$  are the absorption cross section, the heating efficiency and solar energy  
 233 flux at the upper boundary of our domain,  $r = r_u$ , and  $N(r) = \int_r^{r_u} n(\bar{r}) d\bar{r}$ , with constant  
 234  $\varepsilon$  out to  $r_u$ . The transition to a transonic solution with  $r_*$  in the continuum region of the



235 atmosphere was found to occur at  $0.69 < Q_{net}/Q_c < 1.6$ , in agreement with our criterion  
236  $Q_c$  calculated from Equation (10).

237 The threshold for transonic flow can be related to the absorbed energy converted  
238 to heat,  $Q_a$ , by accounting for the non-adiabatic cooling processes,  $Q_{cool}$ :  $Q_{net} \sim Q_a -$   
239  $Q_{cool}$  (Erwin et al. 2013, Figure 4b). If  $Q_{cool}$  is small, writing  $Q_a \sim \varepsilon \pi r_a^2 F_{UV/EUV}$ , then  
240  $\Phi_{EL}$  in Equation (5) can be roughly scaled by the luminosity *if* the solutions are *subsonic*  
241 or do not significantly exceed  $Q_c$ . Because the atmospheric expansion affects  $r_a$ , iterative  
242 solutions can improve estimates of  $Q_a$ . Ignoring this, we note that for an early earth-like  
243 upper atmosphere dominated by N or O, a solar EUV flux more than 100 times the  
244 present would be required for the escaping gas to go sonic in the continuum regime using  
245 data from Tian et al. (2008) in Equation (10). It is, therefore, unlikely that escape from  
246 such an atmosphere on a super-earth in the habitable zone would have a sonic point in the  
247 continuum regime.

248 Lammer et al. (2012) calculated the escape rate from a hydrogen atom  
249 thermosphere due to XUV radiation on super-earths observed orbiting close to their star.  
250 They used Parker's upper boundary conditions to solve the continuum equations and then  
251 decided that blow-off occurred if  $\lambda_x < 3/2$  (Öpik 1963). Rather than solving these  
252 equations and then deciding whether the sonic or Jeans conditions should have been used,  
253 Equation (10) can be used to estimate whether a sonic point might occur in the continuum  
254 regime for a given  $Q_{net}$ .

255 For example, using  $Kn_m \sim 1$  and  $r_* \sim r_0$  we find that  $Q_c \sim 0.6 \times 10^{13}$  W and  
256  $2.5 \times 10^{13}$  W for Kepler11b and 11c respectively, using data in Table 1 of Lammer et al.  
257 (2012). These values can be compared to their heating rates obtained using  $\varepsilon =$   
258 0.15:  $Q_{net} \sim 1.2$  and  $0.3 \times 10^{13}$  W respectively. For this  $\varepsilon$ , Kepler11b has a sonic point  
259 ( $Q_{net} > Q_c$ ) in the continuum region, whereas Kepler11c does not ( $Q_{net} < Q_c$ ).  
260 Therefore,  $\Phi_{EL}$  in Equation (5) is most applicable to Kepler11c which requires kinetic,  
261 not sonic, boundary conditions to obtain for an accurate description of its upper  
262 atmosphere. Of course, increasing  $\varepsilon$  or reducing the gravitational energy due to the tides  
263 can change this.

## 264 Summary

265 We have used results from DSMC simulations to show that the oft-used energy  
266 limited rate in Equation (5) for an isentropic expansion of a heated upper atmosphere is  
267 most reasonable for a subsonic expansion with a large escape rate. The accuracy depends  
268 on how well one estimates  $Q_{net}$ . Conversely, agreement the energy limited escape rate  
269 *does not* imply that sonic boundary conditions are applicable to continuum models of  
270 thermal escape. In fact the simple approximation in Equation (5) becomes less good with  
271 increasing  $Q_{net}$  above  $Q_c$  as seen in Figure 2. Although the *size* of the escape rate might  
272 not be strongly dependent on whether sonic, Jeans, or kinetic boundary conditions are  
273 used, the upper atmosphere can be significantly affected as seen in Figure 3. Therefore,  
274 past applications Parker's (1964a,b) model have led to incorrect descriptions of the upper  
275 atmosphere when rapid escape occurs (Tucker and Johnson 2009; Tucker et al. 2012;  
276 Erwin et al 2013). Since the upper atmosphere structure affects the interaction of the  
277 escaping gas with the ambient plasma and with neighboring bodies, we have given an  
278 expression in Equation (10) to estimate when sonic boundary conditions are likely to be

279 applicable in calculating the escape from and the expansion of the upper atmosphere of a  
280 planetary body.  
281

## 282 **Acknowledgement**

283 We acknowledge support from NASA's Planetary Atmospheres Program

## 284 **Appendix**

285 When  $Q_{net}$  is absorbed in a layer at  $r_a$  and  $u(r)$  is small below  $r_a$ , Equations (1-2)  
286 can be integrated using  $\kappa = \kappa_0(T/T_0)^\omega$  and assuming zero gas velocity below the  
287 heated layer:

$$288 \quad Q_{net} = E^+ + \frac{4\pi\kappa_0 T_0 r_0}{\omega+1} \frac{r_a/r_0}{r_a/r_0-1} \left[ \left( \frac{\lambda_0 r_0}{\lambda_a r_a} \right)^{\omega+1} - 1 \right] + 4\pi r_0^2 n_a \sqrt{\frac{\gamma}{m\lambda_a}} Ma_a \left[ \frac{r_a}{r_0} U(r_0) \right]^{3/2} \frac{r_0/r_a+1}{2},$$

289 where  $Q_{net}$  is lost by energy carried off by escaping molecules,  $E^+$ , by downward  
290 thermal conduction (second term), and by adiabatic cooling (third term). Simulations  
291 having significant escape rates indicate that the last term dominates; assuming  $r_a/r_0 -$   
292  $1 \ll 1$  we obtain Equation (9).

293

294 **References**

- 295 Bird, G.A., 1994. *Molecular Gas Dynamics and the Direct Simulation of Gas Flows*.  
296 Clarendon Press, Oxford, New York.
- 297 Chamberlain, J.W. and D.M. Hunten, *Theory of Planetary Atmospheres*. Academic  
298 Press, NY, 1987
- 299 Erkaev, N.V., [H. Lammer](#), [P. Odert](#), [Yu. N. Kulikov](#), [K. G. Kislyakova](#), [M. L.](#)  
300 [Khodachenko](#), [M. Güdel](#), [A. Hanslmeier](#), [H. Biernat](#), 2012. Part I: Atmospheric  
301 expansion and thermal escape [arXiv:1212.4982](#) 40pages.
- 302 Erwin, J. Erwin, J., O.J. Tucker, R.E. Johnson, 2013 *Icarus* submitted.
- 303 Hunten, D.M., Watson, A.J., 1982. Stability of Pluto's atmosphere. *Icarus* 51, 665– 667.
- 304 Hunten, D. 1982, Thermal and non-Thermal Escape Mechanisms for Terrestrial Bodies.  
305 30, 773-783.
- 306 Johnson, R.E., M.R. Combi, J.L. Fox, W-H. Ip, F. Leblanc, M.A. McGrath, V.I.  
307 Shematovich, D.F. Strobel, J.H. Waite Jr, 2008. Exospheres and Atmospheric  
308 Escape, Chap. in *Comparative Aeronomy*, Ed. A. Nagy, *Space Sci Rev* 139: 355-  
309 397, DOI 10.1007/s11214-008-9415-3.
- 310 Lammer, H. et al., 2009. *Astron. Astrophys.* 506, 399– 410.
- 311 Lammer,H., N. V. Erkaev, P. Odert, K. G. Kislyakova, M. Leitzinger, M. L.  
312 Khodachenko 2012 [arXiv:1210.0793v2](#)
- 313 McNutt, R.L., 1989. *Geophys. Res. Lett.* 16, 1225–1228.
- 314 Murray-Clay, R.A., Chiang, E.I., Murray, N., 2009. *Astrophys. J.* 693, 23–42.
- 315 Opik, E.J., 1963. *Geophys. J. Int.* (1963) 7 (4): 490-509.
- 316 Parker, E.N., 1964a. *Am. Astron. Soc.* 139, 72–92.
- 317 Parker, E.N., 1964b. *Am. Astron. Soc.* 139, 93–122.
- 318 Strobel, D.F., 2008. N<sub>2</sub> escape rates from Pluto's atmosphere. *Icarus* 193, 612–619.
- 319 Tian, F., Kasting, 2008. *J. Geophys. Res.* 113, E05008; doi10.1029/2007JE002946.
- 320 Tucker, O.J., and R.E. Johnson, 2009. Thermally driven atmospheric escape: Monte  
321 Carlo simulations for Titan's atmosphere, *Planetary Space Sci.* 57, 1889-1894.
- 322 Tucker, O.J., J.T. Erwin, J.I. Deighan, A.N. Volkov, R.E. Johnson, 2012, Thermally  
323 driven escape from Pluto's atmosphere: A combined fluid/kinetic model, *Icarus* 217,  
324 408-415.
- 325 Volkov, A.N. and R.E. Johnson 2013 Thermal escape in the hydrodynamic regime:  
326 Reconsideration of Parker's isentropic theory based on results of kinetic  
327 simulations. *Astrophys. J.*, in press.
- 328 Volkov, A.N., Johnson, R.E., Tucker, O.J., Erwin, J.T., 2011a. Thermally-driven  
329 atmospheric escape: Transition from hydrodynamic to Jeans escape. *Astrophys. J.*  
330 729, L24, 1–5
- 331 Volkov, A.N., Johnson, R.E., Tucker, O.J., Erwin, J.T., 2011b. Kinetic simulations of  
332 thermal escape from a single component atmosphere. *Phys. Fluids* 23, 066601, 1–  
333 16.
- 334 Watson, A.J., Donahue, T.M., Walker, J.C.G., 1981. The dynamics of a rapidly escaping  
335 atmosphere: Applications to the evolution of Earth and Venus. *Icarus* 48, 150–166.  
336